

Reinforcement effect of polypropylene fiber on dynamic properties of cemented tailings backfill under SHPB impact loading



Gaili Xue^{a,b}, Erol Yilmaz^c, Guorui Feng^{a,b}, Shuai Cao^d, Lijuan Sun^e

^a College of Mining Technology, Taiyuan University of Technology, Taiyuan 030024, China

^b Research Center of Green Mining Engineering Technology in Shanxi Province, Taiyuan 030024, China

^c Department of Civil Engineering, Geotechnical Division, Recep Tayyip Erdogan University, Fener, Rize TR53100, Turkey

^d School of Civil and Resources Engineering, University of Science and Technology Beijing, Beijing 100083, China

^e State Key Laboratory for Nonlinear Mechanics (LNM), Institute of Mechanics Chinese Academy of Sciences, Beijing 100190, China

HIGHLIGHTS

- Dynamic loadings such as blasting may lead to the failure of backfilling under different strain rates.
- Dynamic properties of cemented tailings backfill (CTB) were examined by the SHPB testing system.
- The original waveform noise of CTB materials with fiber is higher than the one without fiber.
- The dynamic stress-strain curve of CTB with fiber shows a 'double peak' phenomenon.
- The failure mode of CTB without fiber is the instability failure under tension.

ARTICLE INFO

Article history:

Received 17 November 2020

Received in revised form 5 January 2021

Accepted 12 January 2021

Available online 5 February 2021

Keywords:

Cemented tailings backfill

Fiber reinforcement

Waveform properties

Dynamic strength

Failure mode

ABSTRACT

Dynamic loads such as blasting may lead to diverse levels of failure in cemented tailings backfill (CTB) under diverse strain rates and frequency spectral amplitudes. Hence, changes in dynamic properties of filling due to these loads should be studied as a function of strain rates for CTB mixtures. In this study, the dynamic characteristics of CTB samples containing polypropylene fiber contents were examined with the use of split Hopkinson pressure bar (SHPB) system and high speed photography technology. The experimental results illustrate that the backfill has a damping influence on the elastic wave. The original waveform noise of CTB with fiber is higher than the one without fiber, and the average strain rate changes the reflected waveform. The effect is greater than the impact velocity. Secondly, the dynamic strength of CTB with fiber is higher than the static strength, which obeys a great effect of the strain rate. Meanwhile, the backfill (with fiber) stress-strain characteristics show a 'double peak' phenomenon, and the difference between the first and the second peak stresses decreases with increasing fiber content. The failure mode analysis demonstrated that the fiber reinforcement stopped the development of big cracks during the tensile fiber pull-out failure regime. Lastly, the findings of the present study can offer an important reference to the overall design of backfilling regarding the understanding of the good dynamic characteristics and the reduction of operational costs.

© 2021 Elsevier Ltd. All rights reserved.

1. Introduction

As metallic and/or non-metallic mines have entered the state of deep mining in succession, the filling mining method has been used extensively mainly due to some advantages such as high resource extraction [1], constant security [2], and decreased surface tailings disposal requirements [3]. Actually, backfilling is get-

ting imperative for mines due to the trends in mining to mine deeper, enhance ore and water recoveries, rise mining cycle and production, and cut environmental impacts as well as rehabilitation costs [4–6]. All these benefits inevitably lead to the development direction and predictable choice of green mining [7]. Backfilling enhances the overall safety and success of underground mining by augmenting both local and regional stability [8,9]. The cemented backfills such as cemented tailings backfill (CTB) also permit the excavation of ore pillars being left for the mine's stability while avoiding some other serious consequences such as subsidence and collapse [10,11]. It is largely accepted by the mining

E-mail addresses: hnpyxgl@126.com (G. Xue), erol.yilmaz@erdogan.edu.tr (E. Yilmaz), fguorui@163.com (G. Feng), sandy_cao@ustb.edu.cn (S. Cao), sunlj@lnm.imech.ac.cn (L. Sun)

industry that CTB promisingly cuts environmental impacts because of a sharp drop in the creation of acidic waters in comparison with traditional tailings management methods such as tailings impoundments and dams [12,13]. CTB is usually made up of total tailings (with a solid concentration of 65–85 wt%), a lean amount of binding agent (ranges from 2.5% to 12.5% by dry mass), and sufficient mixing water while flowing to underground mined-out stopes [10,14,15]. Rarely, sand and/or chemical admixtures are used to provide a better geotechnical property and structural backfill material [16,17]. It is fairly apparent that any backfill material must keep sufficient mechanical strength for guaranteeing the stability of mine workers and structures throughout the mining of adjacent stopes [18]. However, it should also be kept in mind that the CTB-filled stopes with the relatively low binder are subjected to many stresses from the neighboring rocks and dynamic loads such as blasting and seismic activities which can eventually lead to the failures of the backfill [19]. Experience shows that some pieces from CTB masses fall into the ground freely due to the nature of their fragility structures when extracting the ore in the adjacent stopes. This could escalate ore dilution and decrease productivity and profits [20].

To surge the strength, stiffness, and post-cracking resistance of cementitious backfills, metal, glass, synthetic, and carbon fibers have been introduced recently to the mining industry [21,22]. Basically, the fiber incorporation aims to repair the fragility of materials through the mobilized shear strength along the failure and aims to bridge the internal micro-cracks which are the typical causes of material failures and linked to poor ductility [23]. To capably achieve the crack propagation of cementitious materials and thus enhance their strength and ductility, numerous researchers have launched a series of experimental works on mechanical properties of CTB samples reinforced with fiber [24,25] and other cementitious materials [26–29]. Indeed, Michell and Stone [30] were pioneer researchers who studied the system of fiber reinforcement for the backfill's design to cut cement-related costs. They recorded a considerable drop in cement consumption, offering cost savings for sustainable backfill operations. Zou and Sahito [31] examined the effect of fiber reinforcement on shotcrete performance of CTB. They obtained 59% increase in the flexural strength gain of backfill incorporating polymer fibers. Moreover, some researchers [32–34] showed a strength improvement of fiber-reinforced backfills and found to rise the load-carrying capacity of backfilling.

Essentially, the understanding of the mechanical properties of different backfills get more and more mature and have been the subject of extensive research [35,36]. They not only consider the influence of curing (i.e., time, temperature, and stress) and placement (i.e., drainage, non-drainage, and evaporation) conditions, chemical composition and other internal factors [37,38], but also include other external factors such as stope conditions and rock-backfill interactions as well as multiple spatial scales such as macro, micro, and meso [39,40]. However, the dynamic properties of backfilling have received less attention since they are time-consuming and costly [41]. It is also not correct to better estimate the strength acquisition of CTB-filled stope by static compression testing done on an individual backfill sample [42]. The dynamic strength should be considered for determining the strength gaining of backfill under diverse loads such as blasting, excavation equipment works, and seismic activities [43,44]. Since underground mining is still dominated by the blasting methods, there are a lot of restrictive factors such as mining disturbances, so that the dynamic property of the backfill has been increasingly attracting attention [45]. Considering the CTB's strength characteristics, the SHPB dynamic test system has obvious advantages over the pendulum impact and can fully obtain the dynamic parameters under the impact of different strain rates [46]. Cao et al. [47–49] carried out a dynamic experiment of CTB considering different loading rates and

SHPB impact effects and quantitatively examined relationship between the backfill peak strength and dynamic characteristics. Zhu et al. [50] conducted a dynamic loading impact test of the graded tailings backfill under extraordinary strain rates. As a function of the stress-strain curves achieved under these strain values, they analyzed the backfill's failure by combined numerical simulations. Besides, Tan et al. [51] investigated the stress-strain curves, dynamic strength, and deformation characteristics of multiple cyclic impacts of CTB samples at an impact velocity that does not cause large macro-destruction. Yang et al. [52,53] used a separate SHPB test setup to examine the dynamic characteristics of high-density whole tailings backfill. The stability of the backfill under high strain rates is mainly evaluated by observing the failure degree of CTB after impact testing [54,55]. Earlier research focused on stress-strain curve, peak strength, deformation characteristics and failure mode, and the correlation between the characteristics of the acquired reflection waveform and the structure of the material itself is often ignored [56–60].

The damage mechanism of CTB is similar to that of rock, which belongs to a discontinuous and non-linear fracture process, and the internal damage gradually evolves into macroscopic cracks such as slight rupture, breakage, and crushing [61–64]. Simultaneously, the technique of assisting the study of the dynamic destruction process of the sample combined with high-speed cameras and image processing techniques have been widely recognized [65–67]. The SHPB system is extensively utilized to evaluate the dynamic strength characteristics of concrete/rock [68]. However, being a controlled low-strength cement-based material, CTB has more diverse properties than concrete and rock. It is characterized by low binder contents - economic reasons and very high-water contents - to get the consistency required for pumping [69]. Accordingly, the backfill's dynamic stress-strain responses should be determined by a SHPB test. In this study, an SHPB system with a special experimental apparatus (noise reduction device) is used to perform impact dynamics experiments on fiber-reinforced CTB samples. A high-speed camera is used to better observe the backfill failure. The stress-strain curve of CTB reinforced with fiber was studied by establishing a quantitative relationship between impact velocity, average strain rate, and dynamic strength. Besides, the difference between the impact waveform and the failure modes of CTB reinforced with and without fiber was analyzed.

2. Materials and methods

2.1. Backfill ingredients

The main ingredients utilized in the present study are the whole tailings (without desliming fines), Portland cement 42.5R ('R' signifies the cement having uniaxial compressive strength values of 22 MPa and 42.5 MPa after 3 and 28 days of curing times, respectively), and polypropylene fiber. According to earlier research results [32–34], it is known that the polypropylene fiber has a high reinforcement effect, and the optimal fiber length is found to be 12 mm. The density of polypropylene fiber is 0.91 g/cm³, the tensile strength is 398 MPa, the modulus of elasticity is 3.85 GPa, and the elongation is 28%. Fig. 1 shows size distribution curves of the studied tailings which contain a clay-sized particle (less than 2 μm) of 6% and a fine content of 29% under 20 μm. This ensures that the tailings retain satisfactory mixing water to create the backfill product. From the cumulative and incremental grain size distribution curves, the uniformity ($C_u: D_{60}/D_{10}$) and curvature ($C_c: D_{30}^2/D_{60} \times D_{10}$) coefficients are found to be 14.8 and 1.9, respectively. Consistent with the Canadian mine tailings classification system, the studied tailings can be ordered as a coarse-size product. Moreover, the chemical analyses designated that the tailings

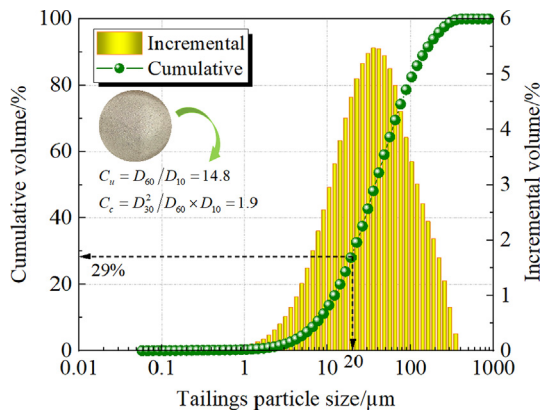


Fig. 1. Particle size distribution curves of the studied tailings sample.

contain a total content of 84% SiO₂, Al₂O₃, CaO, and MgO. According to the JC/T 2478-2018 standard [70], the alkalinity [$M_o = (\text{CaO} + \text{MgO})/(\text{SiO}_2 + \text{Al}_2\text{O}_3)$] displays that the tailings are acid-generating (Table 1).

2.2. Experiment scheme design

Self-made plate pillar molds with a size of $\Phi 50 \text{ mm} \times 30 \text{ mm}$ were used for making CTB samples impacted by an SHPB testing device. The operating system of this device is relied on the theory of 1D wave propagation in an elastic bar. Samples have a cement/tailings (c/t) ratio of 1:6 and 1:8 as well as a solid concentration of 75 wt%. First, the cement-to-tailings ratio was set to 1:6 and 1:8, which is more in line with the actual application requirements of the mine. Secondly, high-concentration slurry can be formed when using whole tailings paste backfill. Finally, based on the previous impact dynamics test results of the research group, it is believed that 75% slurry concentration is easier to obtain a better impact effect [50,51].

Known as a synthetic fiber transformed from 85% propylene, polypropylene fiber is used during the experiments at a content of 0 wt%, 0.3 wt%, 0.6 wt% and 0.9 wt% of dry tailings and cement. The prepared backfill mixtures are kept in a curing room (the temperature: $20 \pm 2 \text{ }^\circ\text{C}$ and the humidity: 95%). The predetermined curing time for all CTB samples is taken as 28-day. Prior to strength testing, the samples' end faces are gently flattened by a cutter. Note that the group format is c/t-concentration-fiber content. For example, 6-75-0.6 means that c/t is 1:6, the slurry concentration is 75 wt%, and the fiber content is 0.6%.

2.3. Experimental equipment and procedures

Fig. 2 shows a view of the SHPB dynamic testing method, which consists typically of a power system, impact/incident/transmission bars, damper, and measurement recording system. The power system mainly refers to the high-pressure nitrogen pushing the impact bar to hit the incident bar at a uniform speed. Strain gauges are affixed at equal distances from the incident/transmission bar to sample to minimize the hysteresis effect of the adhesive on the transmitted signal and the interference of the reflected wave on the stress balance in the sample. Hence, the strain gauges used

are high sensitivity coefficient of semiconductor strain gauges AF2-120. So, incident/transmission bars are 2000 mm in length and 50 mm in diameter, the elastic modulus of two bars is 206 GPa, the bar density is 7900 kg/m³, the longitudinal wave velocity is 5065 m/s, the length of the absorption bar is 1000 mm, and the diameter is 50 mm. The TST3000 acquisition system can store data independently, and the TST3406 high-speed, high-precision dynamic test analyzer collects and processes shock waves. The pulse shape used in this experiment is a sine waveform. A high-speed camera VW-600 M has a sharp resolution of 640×480 pixels, and a dynamic analysis module VW-9000E, which meets the requirements of the image of material during dynamic destruction.

In this study, the size of the impact equipment bar (i.e., diameter and length), the size effect of the backfill sample (the larger the volume, the higher the dispersion of internal cracks, and the lower the strength under the same strain rate), and the effect of backfill settlement on the impact data results were analyzed. Consequently, the impact bar having 50 mm diameter was adopted, and the height/diameter ratio of CTB sample was set at 0.6.

3. Results and discussion

3.1. Dynamic waveform spectral analysis

Fig. 3(a) and (b) demonstrate the discrete voltage indicators of the original incident, and reflected and transmitted waves collected by the waveform collector. As shown in Fig. 3(a), the amplitudes of the incident/reflected waves are equal, but the values are in opposite directions, whereas the amplitude of the transmitted wave is small. The incident bar's elastic modulus is 206 GPa, and the corresponding density is 7800 kg/m³. The backfill sample belongs to the category of soft rock, and its density is less than 2000 kg/m³. The wave impedance capability between the CTB sample and the incident bar is quite different. Most of the stress pulses return to the incident bar, leading to a smaller transmission amplitude of the stress pulse compared with that of the incoming reflected wave, accordingly a strong damping and shielding effect of the backfill on elastic wave propagation.

Second, with the constant rise in impact velocity, the voltage amplitudes of incoming/transmitted waves are increased. The larger is the area enclosed by the x-coordinate, the larger is the impact velocity, and the larger are the incident and reflected energies. When the impact velocities are 2.978 and 2.935 m/s, the average strain rates are 35.969 and 37.761 s⁻¹. When the impact velocities are 2.862 and 2.997 m/s, the average strain rates are 47.828 and 53.004 s⁻¹. At this point, the variation trend of the incident and reflected waves, with average strain rates close to each other, is consistent.

Fig. 3(a) shows the larger number of noise phenomena in the original data of fiber-reinforced CTB compared with those of rock samples [67,71]. The curve is smoothed by the FFT Fourier function filter that has filtered out the high-frequency signal, but Savitzky-Golay convolution smoothing filter algorithm can also eliminate noise interference while retaining an original signal by carrying out polynomial regression on the local data. The initial voltage signal waveform is calibrated according to stress wave theory, and the starting point is selected, then the obtained electrical signal is converted into a strain signal by MATLAB software. The

Table 1
Chemical composition analyses of the tested tailings sample.

Analysis (%)	SiO ₂	Al ₂ O ₃	CaO	MgO	P	Fe	S	Au	Ag	Cu
Value	64.90	13.68	1.92	3.50	0.06	2.80	0.15	<0.01	0.03	<0.01

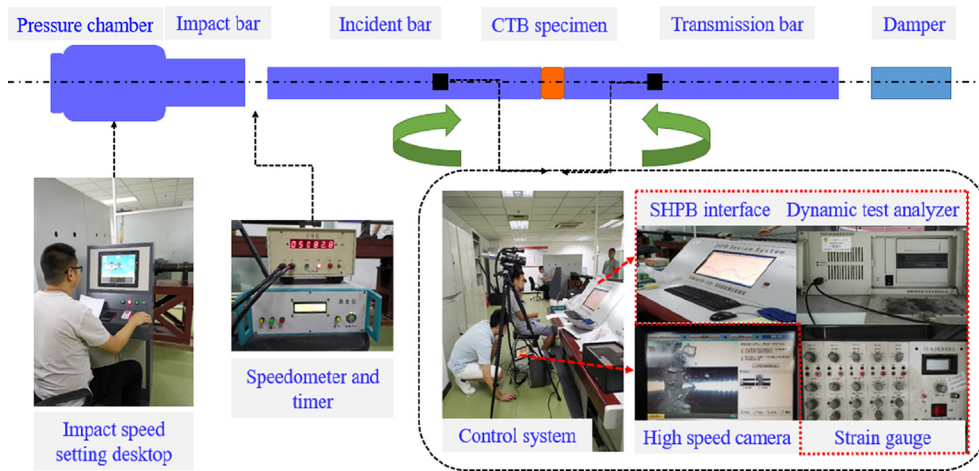


Fig. 2. A schematic illustration of the studied SHPB test apparatus and mechanism.

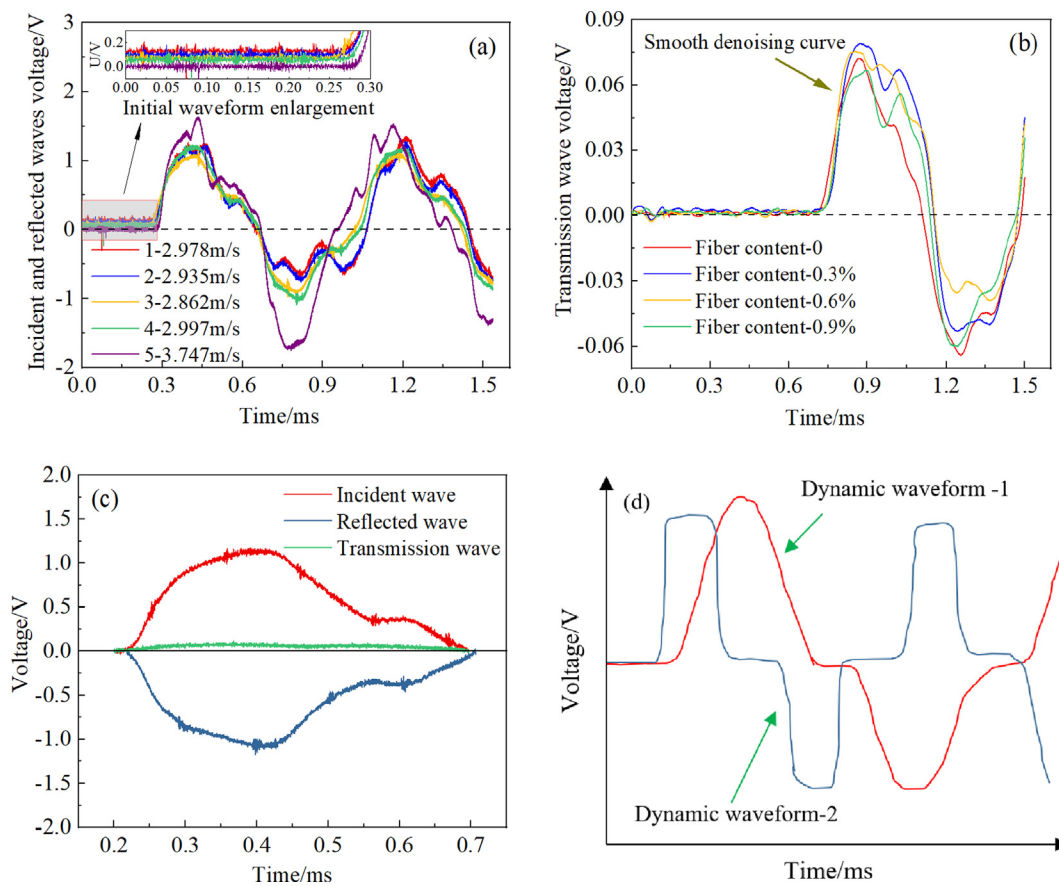


Fig. 3. CTB's dynamic waveform: (a) incident and reflected waves (6-75-0.3); (b) transmission wave with different fiber content-3 m/s; (c) stress wave balance correction; (d) typical dynamic waveform.

smooth denoising curve of transmission wave with different fiber content is shown in Fig. 3(b).

Fig. 3(b) demonstrates that the highest value of the transmission wave shape is clearly correlated to the sample's peak strength under an impact condition of 3 m/s. However, the shapes of the transmitted waves vary greatly, and the fiber-reinforced CTB samples manifest a phenomenon of "double peaks." Meanwhile, the second wave peak of the non-reinforced backfill sample is not obvious, and the duration is relatively shortened. With the incorporation of fiber, the backfill sample can retain the integrity of

the solid core, prolong the action time of stress waves, and slow down the attenuation rate of stress waves owing to the germination and expansion of cracks. This scenario reflects the damage degree of the sample. For example, the failure mode of non-reinforced CTB 6-75-0 is 'crush,' whereas the failure mode of fiber-reinforced CTB 6-75-0.6 takes the integrity of the 'solid core,' and the peripheral is 'peeling broken.'

The stress balance algorithm is used for correction to guarantee the results' precision. Note that the backfill sample 6-75-0.3 is taken as an example. As the considered impact velocity is set to

2.997 m/s, the duration of incident/reflected/transmitted waves is consistent. Fig. 3(c) demonstrates that the curve obtained by superimposing the incident/reflected waves is consistent with that of the transmitted wave. Fig. 3(d) displays that the dynamic waveform spectrum is related to the loading form of the stress wave (semi-sine or rectangular wave), and the time interval between the incident and waves is related to the bullet's length and sample's internal structure. The peak time of the incident wave of backfill 6-75-0.3 is more delayed, and the time interval of the incident and reflected waves is more prolonged, compared with those of the rock mass samples. The round-trip propagation of the stress waves in the rock mass is relatively high when the impact velocity is the same. The stress balance between the two ends is easily realized, and the external interference effect is eliminated [67,72,73].

3.2. Dynamic strength and strain rate effects

3.2.1. Strain rate effect under different impact velocities

Table 2 lists the numerical results of the samples' impact test limits. When the impact velocity is similar (this means that the aggregate, cementing agent, and fiber categories are all the same), and the slurry concentration is 75%, the average value can be obtained from Fig. 4.

The combined findings from Table 2 and Fig. 4 indicate that when the impact velocity is 3 m/s, the dynamic mechanical strength of fiber-reinforced CTB samples 6-75-0, 6-75-0.3, 6-75-

0.6, and 6-75-0.9 are 3.323 MPa, 3.19 MPa, 3.466 MPa, 3.108 MPa, which are higher than its static compressive strength (2.458 MPa, 2.870 MPa, 3.432 MPa, 3.058 MPa [34]). It shows that CTB under dynamic load can yield a higher bearing capacity. The finding conforms with a great effect of strain rate. However, the dynamic increase factor in this experiment is small at 1.02–1.689 only. The reason is that the partially lost cement slurry reduces the total amount of cementation, thus it decreases the hydration products and loosens the filling test block structure, which then affect the proportion of strength growth. In addition, when the impact velocity is the same, the larger the c/t is, the greater the backfill dynamic strength will be. When the c/t is the same, the larger the impact velocity is, the greater the backfill dynamic strength will be.

When the c/t ratio is 1:6, with increasing strain rate, the backfill (with fiber) dynamic strength gain progressively surges, and good correlation is achieved, as shown in Fig. 5(a). When the impact velocities are 2.802 and 2.992 m/s, the average strain rates of CTB 6-75-0 are 55.718 and 61.537 s^{-1} . When the impact velocity is approximately 3 m/s, the backfill (with fiber) strain rate is low, with values mostly below 55 s^{-1} . At the same time, the linear fitting function of dynamic strength and average strain rate of the backfill with different fiber content is obtained. Under the same conditions of cement-sand ratio and slurry concentration, the effect of the strain rate of non-reinforced CTB is more significant than that of CTB with fiber reinforcement.

Table 2
Statistics of impact test parameters of the fiber-reinforced CTB samples.

Group (height to diameter ratio)	Test No.	Specific gravity (g/cm^3)	Impact velocity ($m \cdot s^{-1}$)	Maximum strain rate (s^{-1})	Average strain rate (s^{-1})	Dynamic strength (MPa)	
6-75-0 (0.59)	1	1.875	2.802	92.825	55.718	3.233	
	2	1.889	2.992	99.763	61.537	3.413	
	3	1.854	3.224	87.343	57.726	3.471	
	4	1.923	4.288	128.716	95.308	4.153	
6-70-0 (0.52)	1	1.887	3.057	74.418	49.662	2.620	
	2	1.875	3.160	124.874	78.680	2.765	
8-75-0 (0.56)	1	1.863	3.212	106.954	63.763	2.380	
	2	1.845	4.139	168.862	102.890	2.824	
6-75-0.3 (0.58)	3	1.827	4.322	168.862	107.581	3.473	
	1	1.865	2.978	61.110	35.969	3.032	
	2	1.842	2.935	61.272	37.761	2.917	
	3	1.879	2.862	78.222	47.828	3.159	
	4	1.922	2.997	90.768	53.004	3.653	
	5	1.841	3.747	135.709	85.508	3.981	
6-70-0.3 (0.58)	6	1.857	4.560	128.716	95.308	4.934	
	1	1.786	3.895	85.849	51.024	2.861	
	2	1.822	3.615	94.268	54.593	3.161	
	8-75-0.3 (0.57)	1	1.874	3.377	107.244	71.358	2.463
		2	1.862	4.304	145.307	89.468	3.198
	6-75-0.6 (0.62)	3	1.870	4.296	180.402	112.547	3.257
1		1.848	2.908	51.563	34.508	3.425	
2		1.793	3.158	77.532	45.374	3.377	
6-70-0.6 (0.54)	3	1.872	3.022	98.814	62.624	3.595	
	4	1.855	3.535	76.980	46.111	3.234	
	5	1.861	3.918	140.941	93.009	4.134	
	6	1.872	4.480	130.533	93.995	4.376	
	8-75-0.6 (0.58)	1	1.812	3.952	157.039	106.194	3.270
		2	1.816	3.588	141.744	92.374	3.173
8-75-0.9 (0.55)	1	1.749	3.183	114.249	70.151	2.353	
	2	1.799	3.266	101.881	64.755	2.408	
	3	1.845	3.233	99.899	57.924	2.874	
	4	1.859	3.554	91.664	57.761	2.995	
	5	1.785	4.096	134.988	84.050	3.016	
6-75-0.9 (0.64)	1	1.860	3.004	87.551	50.398	3.108	
	2	1.861	3.566	95.308	69.281	3.523	
	3	1.868	4.081	125.109	80.818	3.943	
8-75-0.9 (0.55)	1	1.776	2.858	99.815	61.993	2.223	
	2	1.760	2.996	93.606	54.017	2.452	
	3	1.767	4.519	172.296	98.573	3.125	
	4	1.737	4.646	173.126	97.502	3.763	

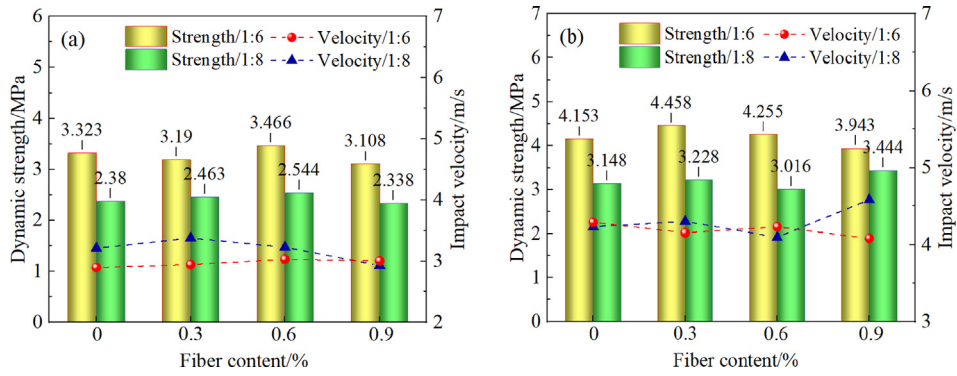


Fig. 4. CTB's dynamic strength with an impact velocity of 3 m/s (a), and 4 m/s (b).

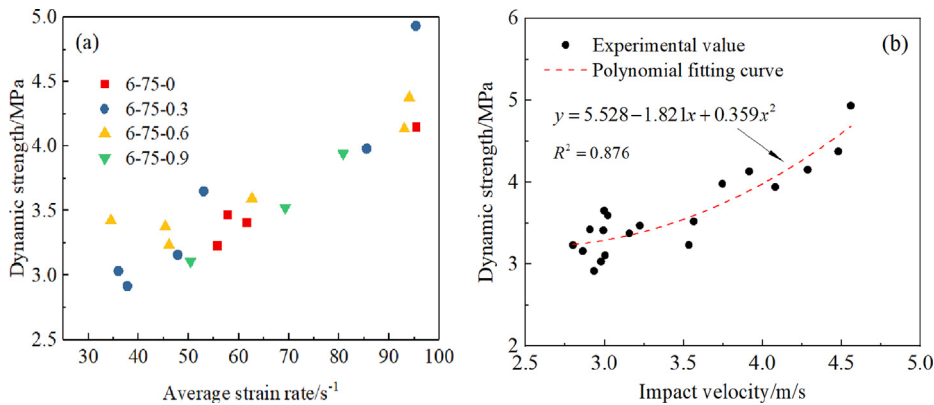


Fig. 5. The backfill (with fiber) strain rate effect: (a) relationship between dynamic strength and strain rate; and (b) relationship between dynamic strength and impact velocity.

Polynomial fitting is performed on backfill's dynamic strength and impact velocity. The complex correlation coefficient is 0.876, and the functional expression is $y = 5.528 - 1.821x + 0.359x^2$. With increasing impact velocity, the backfill's strength trend is also increased, as shown in Fig. 5(b). Under the same impact velocity, the dynamic strength difference between different types of backfills is obvious. The average strain rate distribution of non-reinforced CTB samples is relatively concentrated, whereas the backfill (with fiber) strain rate is discrete, with increasing fiber content. The effect of average strain on the backfill's dynamic strength is pronounced. The impact velocity range adopted in this experiment is small because the average strain rate of the critically unstable non-reinforced CTB samples is approximately 50 s^{-1} [61,62]. If the average strain rate is higher than this value, the backfill tends to be broken and crushed. However, the impact velocity continues to increase considerably in this experimental study, and the dynamic strength of backfilling still has room to improve.

3.2.2. Stress-strain curve analysis

Fig. 6 displays that the backfill's stress-strain curves are similar to the wave shape curve of the transmitted wave, in which 'double peaks' are observed. The compaction effect of the micro-cracks and pores within the sample can be realized quickly under the action of impact load. Therefore, the initial stress-strain curve of backfilling has a good coincidence, and it differs from the quasi-static loading curve. The difference is not reflected in the stress-strain curve of the internal micro-pores. When the CTB sample reaches the first peak stress, the sample begins to show strain softening, and a slight fracture is formed. As the strain value continuously

increases, the micro-cracks under compression manifest strain strengthening when the stress gradually rises to the second peak stress, and the damage evolves into a macro-crack, which represents a sharp decrease in stress.

Second, the first peak stress is greater than the second peak stress, and it tends to decrease with increasing fiber content. Note that the medium strain rate shock loading is taken as an example. The differences between two peak stresses of backfill, particularly 6-75-0, 6-75-0.3, 6-75-0.6, and 6-75-0.9, are 1.468, 0.582, 0.319, and 0.116 MPa. The cracking-resisting and anti-cracking effect of fiber is based on the cement hydration reaction, in which large number of cementitious materials are produced to wrap the fiber, and good integrity with the backfill matrix is achieved. When the slurry concentration and the c/t is the same, the increased incorporation of the fiber content means that more cementitious materials are needed to cover the fiber surface. However, at this time, the percentage of cement content given the same volume is reduced. Thus, the fiber content of the backfill with the same type of cement entails a critical value, which then affects the dynamic strength growth ratio.

CTB is considered as a non-uniform cement-based composite material belonging to the group of strain rate-sensitive materials. Average strain rate can be divided into the following three groups: low, medium, and high strain rates. The maximum strain value of CTB increases with rising strain rate, and the backfill (with fiber) strain value is greater than that of CTB without fiber. The average growth factor of the backfill's dynamic strength is 1 under the loading condition of the low strain rate (50 s^{-1}). At this time, the 'double peak' of the stress-strain curve of non-reinforced CTB 6-75-0 continues to exist. The average growth factor of the dynamic

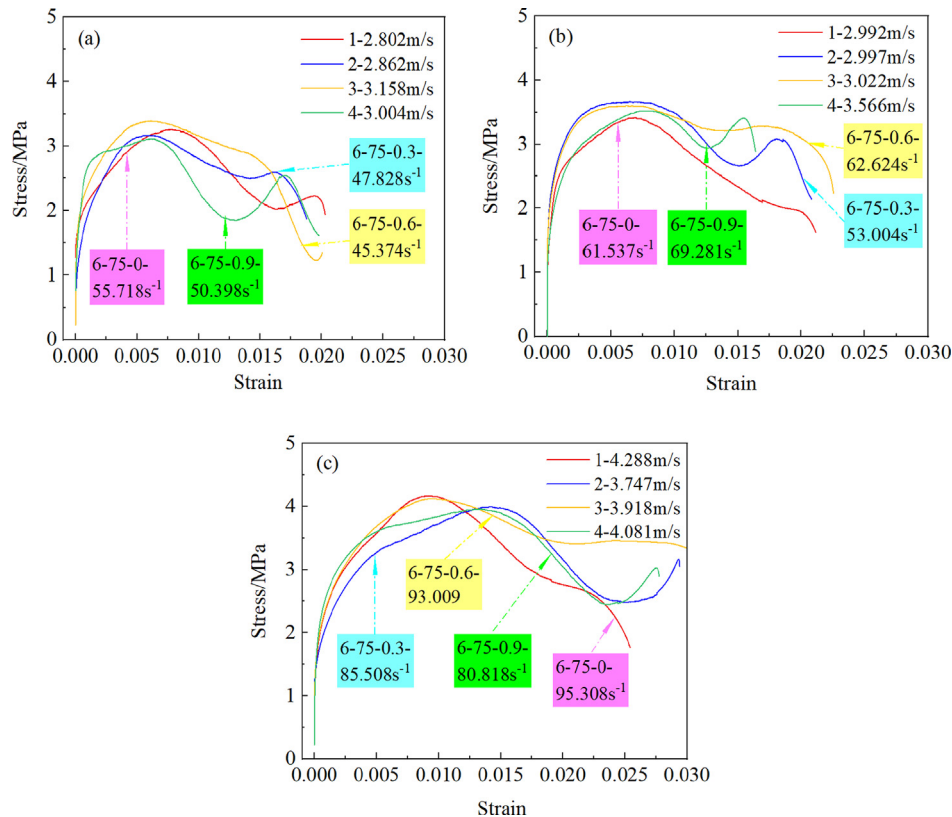


Fig. 6. The backfill (fiber) stress-strain curves under low (a), medium (b), and high (c) strain rates.

strength of CTB is 1.2 under the loading condition of the medium strain rate (approximately 65 s^{-1}). Under the two impact conditions mentioned above, the cracks play the main controlling role, and the first peak stress entails a certain homogeneous action stage. The average growth factor of the dynamic strength of CTB is 1.4 under the loading condition of high strain rate (approximately 90 s^{-1}). The observations from Fig. 6(b) and (c) indicate that non-reinforced CTB sample does not have the second 'peak stress' under the impacts of medium and high strain rates.

The results of high-speed photography are shown in Fig. 7. The bearing structure of non-reinforced CTB sample is damaged when the impact velocity is 2.992 m/s, and its effective loading area is greatly reduced. The strain strengthening cannot be realized through regional stress adjustment alone, as the macroscopic failure of the sample is the dominant control factor. Thus, the backfill's stress-strain curve shows a large downward trend when the strain rate increases to a certain value, and the disappearance of the 'double peak' phenomenon is not an accidental phenomenon. Second, the fiber-reinforced CTB sample differs from the coal sample containing gangue. The interface between gangue and coal in the coal sample has damaged the integrity of the structure [71,72].

The reason is that the interface of coal samples containing gangue is similar to the effect of macroscopic cracks. However, the effective bonding between the fiber and the backfill matrix can induce a surrounding bearing structure. Moreover, even if a local fracture occurs, the backfill can still be reloaded. The backfill sample with a c/t ratio of 1:6 is taken as an example. The fragmentation degree of the CTB sample 6-75-0 increases under the impact velocity of 3 m/s, but a large block rate can be still observed. Meanwhile, fiber-reinforced CTB samples bounce the powder around in a radial direction, whereas the main structure of CTB sample 6-75-0.3 produces several fracture surfaces. The structure of CTB 6-75-0.6 has good structural integrity, which can indirectly explain why its second peak stress is higher than those of other groups.

3.2.3. Dynamic strength response surface

The response surface of the fiber content and the average strain rate relative to the dynamic strength of filling are shown in Fig. 8. The failure pattern of the backfill sample displays that the backfill's dynamic strength and integrity are related to the strain rate. Similarly, with increasing strain rate, the backfill's dynamic strength increases, and the degree of damage changes from good integrity to complete instability. By contrast, under the effect of different slurry concentrations and c/t, the maximum strain rate and dynamic strength under the same impact velocity differ greatly. When the c/t is 1:8, and the impact velocity is 3.2 m/s, the backfill's dynamic strength is approximately 2.4 MPa, and the maximum strain rate can reach 108.062 s^{-1} . The corresponding dynamic strength is only 71.86% of the backfill sample having a c/t ratio of 1:6 (its maximum strain rate is 99.763 s^{-1} , and the average impact velocity is 3.043 m/s).

As the impact velocity is 4.3 m/s, the backfill's dynamic strength is roughly 3.2 MPa, and the maximum strain rate can reach 180.402 s^{-1} . The corresponding dynamic strength is approximately 79.8%, and the highest strain rate is 127.9% of the CTB sample with a c/t of 1:6. Second, under the effect of the same impact strain rate, the backfill (with fiber) dynamic strength is higher than that of CTB without fiber. The main reason behind this behavior is that the incorporation of fiber mainly improves the impact-resistance performance of the backfill, as energy is slowly released along with the effective time of impact load, and the damage to be caused is reduced. Thus it improves the dynamic strength value of CTB. When the c/t ratio is 1:6, the backfill having 0.9% fiber content has a slightly lower dynamic strength under the action of medium strain rate (i.e., zone A in Fig. 8a) compared with the other backfill samples. The crack initiation and propagation are mainly affected by the viscous effect inside the fiber-reinforced backfill material. The backfill with a c/t ratio of 1:8 and 0.9% fiber content has a significantly higher dynamic strength under the action of high strain

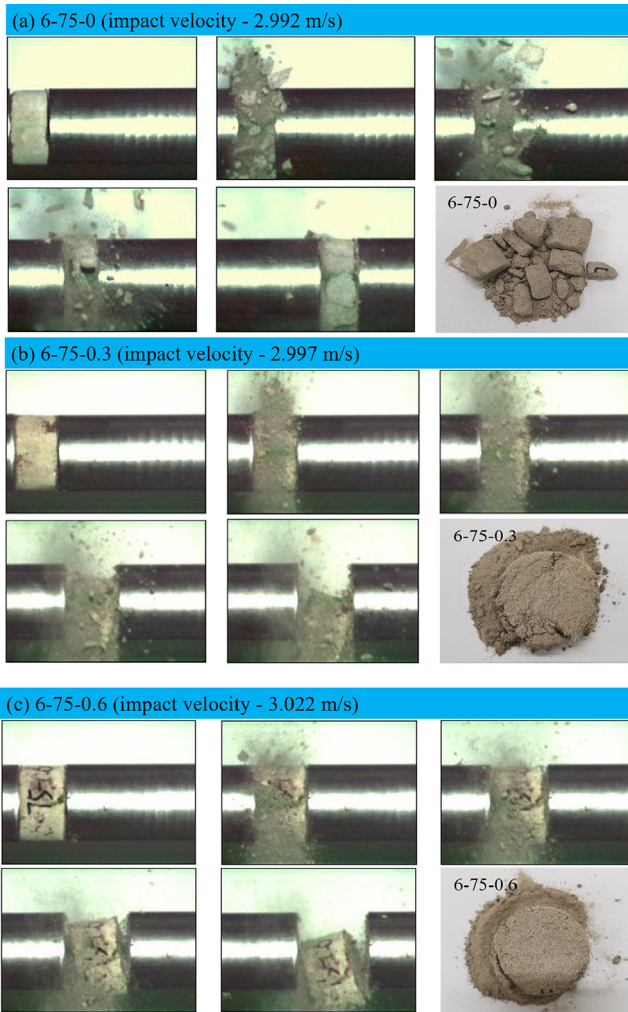


Fig. 7. The failure process of CTB having different fiber contents.

rate (i.e., zone B in Fig. 8b) compared to other backfill samples. The main reasons can be explained as follows: The impact velocity is controlled by adjusting the pressure chamber. When the chamber pressure and the c/t are the same, the maximum impact velocity of sample 8-75-0.9 is 4.6 m/s; the maximum impact velocity of other samples is 4.3 m/s, the minimum value of the maximum impact velocity is 4.1 m/s. The impact velocity is larger, and the inertial effect from the dynamic perspective is substantial. In other words,

if the impact velocity is increased, then the inertial force will increase to improve the backfill dynamic strength.

3.3. Backfill (with fiber) failure characteristics

Limited by this paper's length, only the impact failure patterns of four typical backfill groups are demonstrated in Fig. 9. When the strain rate exceeds 40 s^{-1} , the non-reinforced CTB sample is broken into large blocks, and no residual strength exists. If the strain rate of the same sample is increased, the fragmentation degree will further decrease until the crushing. When the average strain rate is lower than 40 s^{-1} , and the appearance of fiber-reinforced CTB samples is almost complete, the integrity of sample 6-75-0.6 is 96.28% (the average strain rate at this time is 34.508 s^{-1}). When the average strain rate is between 40 and 50 s^{-1} , the elastic powder in fiber-reinforced CTB is intensified. As the average strain rate is between 50 and 70 s^{-1} , the elastic powder begins to peel off around the two end faces of backfill (with fiber).

The backfill's stability is damaged due to the occurrence of partial through-penetration cracks. However, the cemented tailings backfill sample continues to retain an intact center and is able to bear plastic deformation, both to a certain extent. As the average strain rate is greater than 70 s^{-1} , the backfill (with fiber) sample becomes unstable. The integrity of the CTB sample 8-75-0.6 is 58.95%, when the average strain rate is 70.151 s^{-1} .

In summary, the failure form of non-reinforced CTB samples is mainly in the form of unstable crushing under tension force, whereas that of fiber-reinforced CTB samples under the impact loading is reflected as edge-spalling, core-retaining, and instability failures.

4. Conclusions

In this study, the SHPB impact test system and high-speed camera technology were employed to investigate the backfill (with fiber) dynamic strength behavior at different impact velocities. From the conducted experiments, some conclusions can be obtained below:

- Either increasing the c/t or decreasing the fiber content can help reduce the noise of the original impact waveform of the fiber-reinforced CTB sample. Second, the transmitted wave of the fiber-reinforced CTB sample has the characteristic of double peaks, and the amplitude of the transmitted wave is positively correlated with its dynamic peak strength.
- Influence of average strain rate on variation trend of the incident and reflected wave shape is greater than that of impact velocity.

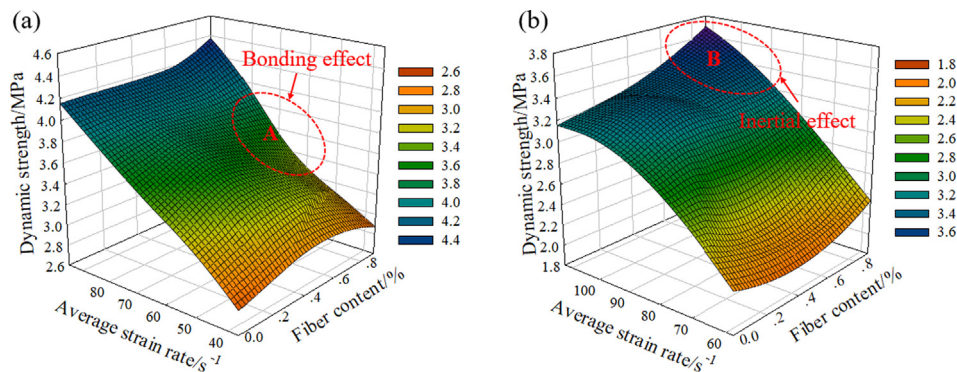


Fig. 8. Response surface of fiber content and average strain rate relative to dynamic strength of the fiber-reinforced CTB: (a) the c/t is 1:6; and (a) the c/t is 1:8.





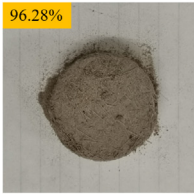

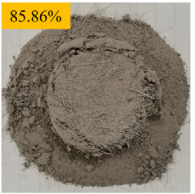
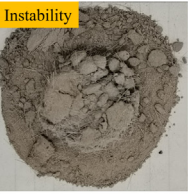

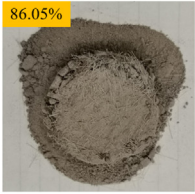
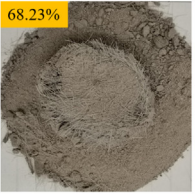


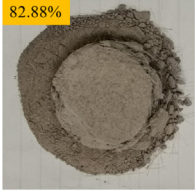
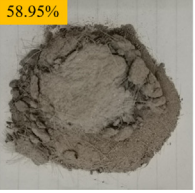

Sample	-	A: average strain rate; B: failure modes of fiber-reinforced CTB samples			
6-75-0	A	40.353 s ⁻¹	55.718 s ⁻¹	61.537 s ⁻¹	95.308 s ⁻¹
	B				
6-75-0.6	A	34.508 s ⁻¹	45.374 s ⁻¹	62.624 s ⁻¹	93.009 s ⁻¹
	B				
6-75-0.9	A	50.398 s ⁻¹	69.281 s ⁻¹	80.818 s ⁻¹	95.308 s ⁻¹
	B				
8-75-0.6	A	42.864 s ⁻¹	57.924 s ⁻¹	70.151 s ⁻¹	84.050 s ⁻¹
	B				

Fig. 9. The backfill (with fiber) failure modes under the impact of different strain rates.

- The backfill (with fiber) dynamic strength is greater than the static compressive strength, and it rises with increasing impact velocity. This finding accords with the law of strain rate effect.
- When the c/t and the slurry concentration are the same, the average strain rate distribution of backfill under similar impact velocity become relatively concentrated, and the strain rate effect is relatively significant.
- The backfill (with fiber) adhesion and fibers can induce a peripheral bearing structure and delay the reduction of the effective bearing area. The corresponding stress-strain curve appears as a double peak, and the difference between the first and second peak stresses decreases with rising fiber content.
- The backfill failure under the action of different impact velocities is in the form of instability failure led by tension, whereas those of CTB with fiber is in the form of edge peeling and core and instability failures, which have secondary bearing capacity at low and medium strain rates and can resist cyclic impact. Thus, the integrity of the backfill samples can be improved.

CRedit authorship contribution statement

Gaili Xue: Conceptualization, Methodology, Formal analysis, Writing - review & editing, Writing - original draft. **Erol Yilmaz:**

Validation, Methodology, Writing - review & editing. **Guorui Feng:** Visualization, Investigation, Writing - review & editing. **Shuai Cao:** Investigation, Methodology, Visualization, Writing - review & editing. **Lijuan Sun:** Investigation, Visualization, Writing - review & editing.

Declaration of Competing Interest

The authors declare that they have no known competing financial interests or personal relationships that could have appeared to influence the work reported in this paper.

Acknowledgements

The authors would like to sincerely thank the National Natural Science Foundation of China (Grant 51804017), the Opening fund of State Key Laboratory of Nonlinear Mechanics (Grant No. LNM202009) and the Fundamental Research Funds for the Central Universities (Grant No. FRF-TP-20-001A2) for their generous financial support to realize this present work.

References

- [1] B.C. Balusa, A.K. Gorai, Sensitivity analysis of fuzzy-analytic hierarchical process (FAHP) decision-making model in selection of underground metal mining method, *J. Sustainable Min.* 18 (1) (2019) 8–17.
- [2] S. Cao, W.D. Song, E. Yilmaz, Influence of structural factors on uniaxial compressive strength of cemented tailings backfill, *Constr. Build. Mater.* 174 (2018) 190–201.
- [3] C. Qi, Q. Chen, A. Fourie, X. Tang, Q. Zhang, X. Dong, Y. Feng, Constitutive modelling of cemented paste backfill: a data-mining approach, *Constr. Build. Mater.* 197 (2019) 262–270.
- [4] W. Li, M. Fall, Strength and self-desiccation of slag-cemented paste backfill at early ages: Link to initial sulphate concentration, *Cem. Concr. Compos.* 89 (2018) 160–168.
- [5] B. Yan, E. Yilmaz, Analytical solution for stress distribution in cementitious backfills considering stope inclinations, *Recep Tayyip Erdogan Univ. J. Sci. Eng.* 1 (2) (2020) 26–33.
- [6] H.Q. Jiang, J. Han, Y. Li, E. Yilmaz, Q. Sun, J. Liu, Relationship between ultrasonic pulse velocity and uniaxial compressive strength for cemented paste backfill with alkali-activated slag, *Nondestruct. Test. Eval.* 35 (4) (2020) 359–377.
- [7] A. Roshani, M. Fall, Rheological properties of cemented paste backfill with nano-silica: link to curing temperature, *Cem. Concr. Compos.* 114 (2020) 103785.
- [8] D. Wu, R. Zhao, C. Xie, S. Liu, Effect of curing humidity on performance of cemented paste backfill, *Int. J. Miner. Metall. Mater.* 27 (2020) 1046–1053.
- [9] B. Koohestani, Mokhtari, E. Yilmaz, F. Mahdipour, A.K. Darban, Geopolymerization mechanism of binder-free mine tailings by sodium silicate, *Constr. Build. Mater.* 268 (2021) 121217.
- [10] S. Zhang, L. Yang, F. Ren, J. Qiu, H. Ding, Rheological and mechanical properties of cemented foam backfill: effect of mineral admixture type and dosage, *Cem. Concr. Compos.* 112 (2020) 103689.
- [11] S. Cao, G.L. Xue, E. Yilmaz, Z. Yin, Assessment of rheological and sedimentation characteristics of fresh cemented tailings backfill slurry, *Int. J. Min. Reclamation Environ.* (2020) 1–17, <https://doi.org/10.1080/17480930.2020.1826092> (in press).
- [12] W. Xu, Y. Zhang, X. Zuo, M. Hong, Time-dependent rheological and mechanical properties of silica fume modified cemented tailings backfill in low temperature environment, *Cem. Concr. Compos.* 114 (2020) 103804.
- [13] B. Yan, W. Zhu, C. Hou, E. Yilmaz, M. Saadat, Characterization of early age behavior of cemented paste backfill through the magnitude and frequency spectrum of ultrasonic P-wave, *Constr. Build. Mater.* 249 (2020) 118733.
- [14] M. Benzaazoua, T. Belem, E. Yilmaz, Novel lab tool for paste backfill, *Can. Min. J.* 127 (3) (2016) 31–33.
- [15] E. Yilmaz, T. Belem, M. Benzaazoua, One-dimensional consolidation parameters of cemented paste backfill, *Miner. Resour. Manage.* 28 (4) (2012) 29–45.
- [16] S.K. Behera, C.N. Ghosh, D.P. Mishra, P. Singh, K. Mishra, J. Buragohain, K. Mandal Phaniil, Strength development and microstructural investigation of lead-zinc mill tailings-based paste backfill with fly ash as alternative binder, *Cem. Concr. Compos.* 109 (2020) 103553.
- [17] J.P. Qiu, Z.B. Guo, L. Yang, H.Q. Jiang, Y.L. Zhao, Effects of packing density and water film thickness on the fluidity behaviour of cemented paste backfill, *Power Technol.* 359 (2019) 27–35.
- [18] J. Li, E. Yilmaz, S. Cao, Influence of solid content, cement/tailings ratio, and curing time on rheology and strength of cemented tailings backfill, *Minerals* 10 (10) (2020) 922.
- [19] E. Yilmaz, T. Belem, M. Benzaazoua, A. Kesimal, B. Ercikdi, F. Cihangir, Use of high-density paste backfill for safe disposal of copper/zinc mine tailings, *Miner. Resour. Manage.* 27 (3) (2011) 81–94.
- [20] H.Q. Jiang, H. Yi, E. Yilmaz, S. Liu, J. Qiu, Ultrasonic evaluation of strength properties of cemented paste backfill: Effects of mineral admixture and curing temperature, *Ultrasonics* 100 (2020) 105983.
- [21] S. Cao, E. Yilmaz, Z. Yin, G.L. Xue, W.D. Song, L. Sun, CT scanning of internal crack mechanics and strength behavior of cement-fiber-tailings matrix composites, *Cem. Concr. Compos.* 116 (2021) 103865.
- [22] B. Koohestani, A.K. Darban, P. Mokhtari, E. Yilmaz, E. Darezeshki, Comparison of different natural fibers treatments – a literature review, *Int. J. Environ. Sci. Technol.* 16 (1) (2019) 629–642.
- [23] L. Festugato, A. Fourie, N.C. Consoli, Cyclic shear response of fiber-reinforced cemented paste backfill, *Geotech. Lett.* 3 (2013) 5–12.
- [24] N.C. Consoli, A. Thome, V. Girardello, C.A. Ruver, Uplift behavior of plates embedded in fiber-reinforced cement stabilized backfill, *Geotext. Geomembr.* 35 (2012) 107–111.
- [25] S. Cao, G.L. Xue, E. Yilmaz, Flexural behavior of fiber reinforced cemented tailings backfill under three-point bending, *IEEE Access* 7 (1) (2019) 139317–139328.
- [26] D.-Y. Yoo, N. Banthia, Impact resistance of fiber-reinforced concrete – a review, *Cem. Concr. Compos.* 104 (2019) 103389.
- [27] N. Banthia, C. Yan, K. Sakai, Impact resistance of fiber reinforced concrete at subnormal temperatures, *Cem. Concr. Compos.* 20 (5) (1998) 393–404.
- [28] D.-Y. Yoo, N. Banthia, Mechanical properties of ultra-high-performance fiber-reinforced concrete: a review, *Cem. Concr. Compos.* 73 (2016) 267–280.
- [29] G.L. Xue, E. Yilmaz, W. Song, S. Cao, Fiber length effect on strength properties of polypropylene fiber reinforced cemented tailings backfill specimens with different sizes, *Constr. Build. Mater.* 241 (2020) 118113.
- [30] R.J. Mitchell, D. Stone, Stability of reinforced cemented backfills, *Can. Geotech. J.* 24 (1987) 189–197.
- [31] D.H. Zou, W. Sahito, Suitability of mine tailings for shotcrete as a ground support, *Can. J. Civ. Eng.* 31 (2004) 632–636.
- [32] G.L. Xue, E. Yilmaz, W. Song, S. Cao, Analysis of internal structure behavior of fiber reinforced cement-tailings matrix composites through X-ray computed tomography, *Compos. B Eng.* 175 (2019) 107091.
- [33] G.L. Xue, E. Yilmaz, W.D. Song, S. Cao, Mechanical, flexural and microstructural properties of cement-tailings matrix composites: effects of fiber type and dosage, *Compos. B Eng.* 172 (2019) 131–142.
- [34] G.L. Xue, E. Yilmaz, W.D. Song, E. Yilmaz, Influence of fiber reinforcement on mechanical behavior and microstructural properties of cemented tailings backfill, *Constr. Build. Mater.* 213 (2019) 275–285.
- [35] Y. Tan, K. Zhang, X. Yu, W.D. Song, J. Wang, C. Hai, The mechanical and microstructural properties of composite structures made of a cement-tailing backfill and rock core, *Minerals* 10 (2) (2020) 159.
- [36] L. Liu, Z. Fang, C. Qi, B. Zhang, L. Guo, K.-L. Song, Experimental investigation on the relationship between pore characteristics and unconfined compressive strength of cemented paste backfill, *Constr. Build. Mater.* 179 (2018) 254–264.
- [37] G.L. Xue, E. Yilmaz, W.D. Song, S. Cao, Compressive strength characteristics of cemented tailings backfill with alkali-activated slag, *Appl. Sci.* 8 (9) (2018) 1537.
- [38] B. Liu, Y.-T. Gao, A.-B. Jin, X. Wang, Dynamic characteristics of superfine tailings-blast furnace slag backfill featuring filling surface, *Constr. Build. Mater.* 242 (2020) 118173.
- [39] I. Cavusoglu, E. Yilmaz, A.O. Yilmaz, Additivity effect on fresh and hardened properties of cemented coal fly ash backfill containing water-reducing admixtures, *Constr. Build. Mater.* 267 (2021) 121021.
- [40] J. Li, E. Yilmaz, S. Cao, Influence of solid content, cement/tailings ratio and curing time on rheology and strength of cemented tailings backfill, *Minerals* 10 (10) (2020) 922.
- [41] L. Yang, W. Xu, E. Yilmaz, Q. Wang, J. Qiu, A combined experimental and numerical study on the triaxial and dynamic compression behavior of cemented tailings backfill, *Eng. Struct.* 219 (2020) 110957.
- [42] S. Cao, G.L. Xue, E. Yilmaz, Y. Zhenyu, Y. Fudou, Utilizing concrete pillars as an environmental mining practice in underground mines, *J. Clean. Prod.* 278 (2021) 123433.
- [43] Y.-H. Zhang, X.-M. Wang, C. Wei, Q.-L. Zhang, Dynamic mechanical properties and instability behavior of layered backfill under intermediate strain rates, *Trans. Nonferrous Met. Soc. China* 27 (7) (2017) 1608–1617.
- [44] Q. Sun, B. Li, S. Tian, C. Cai, Y. Xia, Creep properties of geopolymer cemented coal gangue-fly ash backfill under dynamic disturbance, *Constr. Build. Mater.* 191 (2018) 644–654.
- [45] K.-W. Xia, Y. Wei, Dynamic rock tests using split Hopkinson (Kolsky) bar system – A review, *J. Rock Mech. Geotech. Eng.* 7 (1) (2015) 27–59.
- [46] S. Cao, E. Yilmaz, G.L. Xue, W.D. Song, Assessment of acoustic emission and triaxial mechanical properties of rock-cemented tailings matrix composites, *Adv. Mater. Sci. Eng.* 6742392 (2019) 12p, <https://doi.org/10.1155/2019/6742392>.
- [47] S. Cao, Research on Structural Characteristics and Dynamic Effect of Cemented Tailings Backfilling and its Application, University of Science and Technology Beijing, Beijing, 2017.
- [48] S. Cao, G.L. Xue, W.D. Song, Q. Teng, Strain rate effect on dynamic mechanical properties and microstructure of cemented tailings composites, *Constr. Build. Mater.* 247 (2020) 118537.
- [49] P.R. Zhu, W.D. Song, L. Xu, J. Wang, F. Wan, A study on mechanical properties of CTBs under impact compressive loading, *J. Vib. Shock* 37 (12) (2018) 131–137.
- [50] Y. Tan, J. Wang, W.D. Song, L. Xu, S. Cao, Experimental study on mechanical properties of cemented tailings backfill under cycle dynamic loading test, *J. Min. Saf. Eng.* 36 (1) (2019) 184–190.
- [51] W. Yang, Q. Zhang, S. Yang, X. Wang, Mechanical property of high concentration total tailing CTBing under dynamic loading, *J. Central South Univ. (Sci. Technol.)* 48 (1) (2017) 156–161.
- [52] W. Yang, M. Tao, X. Li, G. Li, Mechanical properties of the total tailing CTBing impacted by cement-sand ratio under high strain rate, *J. Northeastern Univ. (Nat. Sci.)* 38 (11) (2017) 1659–1663.
- [53] M. Wang, Z. Zhu, X. Wang, The growth of mixed-mode I/II crack under impacting loads, *Chin. J. Rock Mech. Eng.* 35 (7) (2016) 1323–1332.
- [54] Y. Zhao, S. Gong, X. Hao, Y. Peng, Y. Jiang, Effects of loading rate and bedding on the dynamic fracture toughness of coal: laboratory experiments, *Eng. Fract. Mech.* 178 (2017) 375–391.
- [55] S. Avachat, M. Zhou, High-speed digital imaging and computational modeling of hybrid metal-composite plates subjected to water-based impulsive loading, *Exp. Mech.* 56 (4) (2016) 545–567.
- [56] A. Nabati, T. Ghanbari-Ghazijahani, C.-T. Ng, CFRP-reinforced concrete-filled steel tubes with timber core under axial loading, *Compos. Struct.* 217 (2019) 37–49.
- [57] M. Tony, T. Su, R. Des, C. David, Finite element modelling of FRP strengthened restrained concrete slabs, *Eng. Struct.* 187 (2019) 101–119.
- [58] A.C. Bhogayata, N.K. Arora, Workability, strength, and durability of concrete containing recycled plastic fibers and styrene-butadiene rubber latex, *Constr. Build. Mater.* 180 (2018) 382–395.
- [59] G. Silva, S. Kim, R. Aguilar, J. Nakamatsu, Natural fibers as reinforcement additives for geopolymers – a review of potential eco-friendly applications to the construction industry, *Sustain. Mater. Technol.* 23 (2020) e00132.

- [60] H.Q. Jiang, M. Fall, E. Yilmaz, L. Yang, L. Ren, Effect of mineral admixtures on flow properties of fresh cemented paste backfill: assessment of time dependency and thixotropy, *Powder Technol.* 372 (2020) 258–266.
- [61] C. Jiao, X. Li, C. Cheng, C. Li, Dynamic damage constitutive relationship of high strength concrete based on fractal theory, *Explos. Shock Waves* 38 (4) (2018) 925–930.
- [62] D. Li, P. Xiao, Z. Han, Q. Zhu, Mechanical and failure properties of rocks with a cavity under coupled static and dynamic loads, *Eng. Fract. Mech.* 225 (2020) 106195.
- [63] Z. Ye, *New Composite Protective Materials of the Dynamic Static Mechanical Properties and Engineering Application*, University of Science and Technology of China, Beijing, 2018.
- [64] D. Ai, Y. Zhao, Q. Wang, C. Li, Experimental and numerical investigation of crack propagation and dynamic properties of rock in SHPB indirect tension test, *Int. J. Impact Eng.* 126 (2019) 135–146.
- [65] T. Lv, *Studies on the Shock Compression Behaviors of Concrete and Steel Reinforced Concrete based on the Split Hopkinson Pressure Bar*, University of Science and Technology of China, Beijing, 2018.
- [66] S.F. Wu, *Study on Impact Damage and Damage Evolution of Siliceous Siltstone of Weiyuan*, China University of Mining and Technology Beijing, Beijing, 2017.
- [67] E. Li, J. Zhou, X. Shi, D.J. Armaghani, Z. Yu, X. Chen, P. Huang, Developing a hybrid model of salp swarm algorithm-based support vector machine to predict the strength of fiber-reinforced cemented paste backfill, *Eng. Comput.* (2020), <https://doi.org/10.1007/s00366-020-01014-x>.
- [68] Q. Zhang, W. Yang, S. Yang, X. Wang, Test research on stability of high-density total tailing CTBing under dynamic loading, *China Safety Sci. J.* 25 (3) (2015) 78–82.
- [69] JC/T 2478-2018, *Tailings Concrete for Mine Goaf Filling*, The Ministry of Industry and Information Technology of the People's Republic of China, Beijing.
- [70] H.T. Li, C.X. Jiang, Y.D. Jiang, H.W. Wang, H.B. Liu, Mechanical behavior and mechanism analysis of coal samples based on loading rate effect, *Int. China Univ. Min. Technol.* 44 (3) (2015) 430–436.
- [71] W. Wang, Experimental study on the mechanical response of water-saturated coal samples under coupled static-dynamic loading, *Henan Polytech. Univ.* (2016).
- [72] H. Lu, *Research on Dynamic Responses and Damage Effect of Red Sandstone with Fluid-Solid Coupling under Impact Loading*, China University of Mining and Technology Beijing, Beijing, 2013.
- [73] K.W. Xia, S. Wang, Y. Xu, R. Chen, B.B. Wu, Advances in experimental studies for deep rock dynamics, *Chin. J. Rock Mech. Eng.* (2021), <https://doi.org/10.13722/j.cnki.jrme.2020.0343>.